Available online at www.sciencedirect.com
ScienceDirect
Optical Materials 29 (2006) 65–69
OPTICAL Materials
www.elsevier.com/locate/optmat

Synthesis and optical properties of ZnO nanostructures with different morphologies

U. Pal [a,*], J. Garcia Serrano [a], P. Santiago [b], Gang Xiong [c,d], K.B. Ucer [d], R.T. Williams [d]

[a] Instituto de Física, Universidad Autónoma de Puebla, Apdo. Postal J-48, Puebla, Pue. 72570, Mexico
[b] Instituto de Física, Universidad Nacional Autónoma de México, A.P. 20-365, C.P. 01000, México D.F., Mexico
[c] Pacific Northwest National Laboratory, P.O. Box 999, K8-88, Richland, WA 99352, USA
[d] Department of Physics, Wake Forest University, Winston Salem, NC 27109, USA

Available online 18 April 2006

Abstract

ZnO nanostructures with different morphologies were grown by a low-temperature hydrothermal technique. The morphology, crystallinity and defect content in the nanostructures could be controlled by adjusting the synthesis conditions. Nanostructures prepared with optimum growth conditions were of good structural and optical qualities. Effects of growth conditions and thermal annealing on the optical properties of the nanostructures were studied by Raman and photoluminescence spectroscopy techniques. It is found that the nanostructures grown with particular initial and final pH values of the reaction mixture and air-annealed at about 250 °C are of best crystalline and optical quality.

Keywords: Zinc oxide; Nanostructures; Optical properties

1. Introduction

Semiconductor nanostructures of desired dimension and morphology are critical for the fabrication of optoelectronic devices. Zinc oxide is a direct band gap semiconductor (3.37 eV at room temperature) and has large exciton binding energy (60 meV) with applications in the fields such as near-ultraviolet emission [1], gas and piezoelectric sensing [2,3], and as transparent electrode material for solar cells [4]. The optoelectronic properties of ZnO nanostructures depend strongly on their morphology, crystalline structure, defect and impurity contents. While several physical methods like vapor-phase epitaxy [5], vapor–liquid–solid growth [6,7], vapor transport [8] and chemical methods like template-assisted growth [9] and solution growth [10,11] have been used to prepare ZnO nanostructures of different morphologies and of good structural and/or optical qualities, there are only a few reports on the synthesis of ZnO nanostructures of good structural and optical qualities through low-temperature synthesis process.

Here we report the synthesis of ZnO nanostructures of different morphologies via low-temperature hydrothermal process with excellent reproducibility. The structure and composition of the nanostructures were studied by X-ray diffraction (XRD), scanning electron microscopy (SEM), energy dispersive spectroscopy (EDS), transmission electron microscopy (TEM) and high resolution electron microscopy (HREM) techniques. The optical properties were studied by Raman and photoluminescence spectroscopy. Our study show that the nanostructures are of good crystalline quality with low structural and electronic defect contents. Air annealing of as-grown nanostructures at 250 °C for 2 h further improves their structural and optoelectronic properties.

* Corresponding author. Tel.: +52 222 295500; fax: +52 222 295611.
E-mail address: upal@sirio.ifuap.buap.mx (U. Pal).

0925-3467/$ - see front matter © 2006 Elsevier B.V. All rights reserved.
doi:10.1016/j.optmat.2006.03.015

2. Experimental

ZnO nanostructures were synthesized through a low-temperature hydrothermal process using ethylenediamine and water (1:9 v/v) as solvent. The morphology of the nanostructures was controlled by adjusting the initial and final pH values of the reaction mixture. While the initial pH of the reaction mixture was controlled through the addition of different amounts of zinc acetate [$(CH_3COO)_2$-$Zn \cdot 2H_2O$] (Baker) in the solvent, the final pH value was controlled by adding different amounts of NaOH (Aldrich, 99%) in it. The final mixture was heated in a round bottom flux between 80 and 100 °C under agitation and kept at this temperature for 2 h. After cooling to room temperature, the white precipitate was filtered and washed by deionized water several times. The details of the sample preparation conditions and the obtained morphologies are reported in [12]. Some of the as-grown samples were annealed in air at various temperatures for 2 h in a horizontal tube furnace.

A Jeol JSM 5600LV scanning electron microscope (SEM) with analytic attachments was used to study the morphology and composition of the nanostructures. Monochromatic Cu K_α radiation from a Phillips (X'Pert) diffractometer was used to record the diffraction pattern of the samples. For transmission electron microscopy (TEM) study, the powder samples were dispersed in water, spread over carbon coated microscopic copper grids, and dried before TEM analysis using a Jeol FEG 2010 FasTem electron microscope.

For room-temperature photoluminescence (PL) measurements, a mode-locked Ti:Sapphire laser operated at the wavelength of 210 nm (the fourth harmonic) was used. The pulse duration was around 150 fs at 76 MHz repetition rate. Typical average beam power at the sample surface was about 2 mW or 6.4 W/cm^2 when focused to a 200 μm spot. A Perkin Elmer NIR Spectrum GX FT-Raman spectrometer with a Nd-YAG laser source (1064 nm) with incident laser power of 2000 mW was used for recording Raman spectra of the samples at room temperature.

3. Results and discussion

The ZnO nanostructures prepared with different initial and final pH values had different morphologies. In Fig. 1, the typical morphologies of the samples revealed by SEM are presented. While the samples prepared with $pH_i = 8.6$ and $pH_f = 10.0$ revealed particle-like morphology, the samples prepared with $pH_i = 9.0$ and $pH_f = 11.0$ revealed flower-like morphology. The samples prepared with $pH_i = 10.0$ and $pH_f = 12.0$ or $pH_i = 11.0$ and $pH_f = 12.0$ revealed inhomogeneous and homogeneous nanorod structures respectively.

The XRD patterns of all the samples revealed a hexagonal wurtzite phase of well crystalline ZnO. In Fig. 2, the XRD patterns of the samples prepared with different initial and final pH values are presented. The diffraction patterns

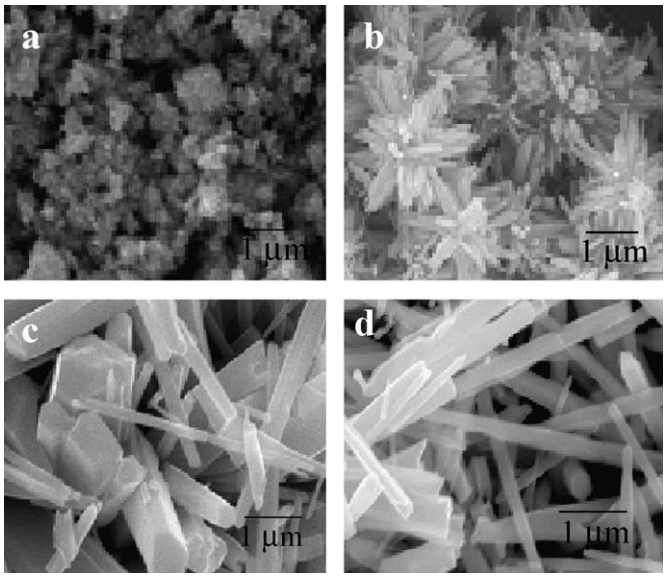

Fig. 1. Typical SEM morphologies of the ZnO nanostructures prepared with (a) $pH_i = 8.6$ and $pH_f = 11.0$, (b) $pH_i = 9.0$ and $pH_f = 11.0$, (c) $pH_i = 10.0$ and $pH_f = 12.0$, and (d) $pH_i = 11.0$ and $pH_f = 12.0$ of the reaction mixture.

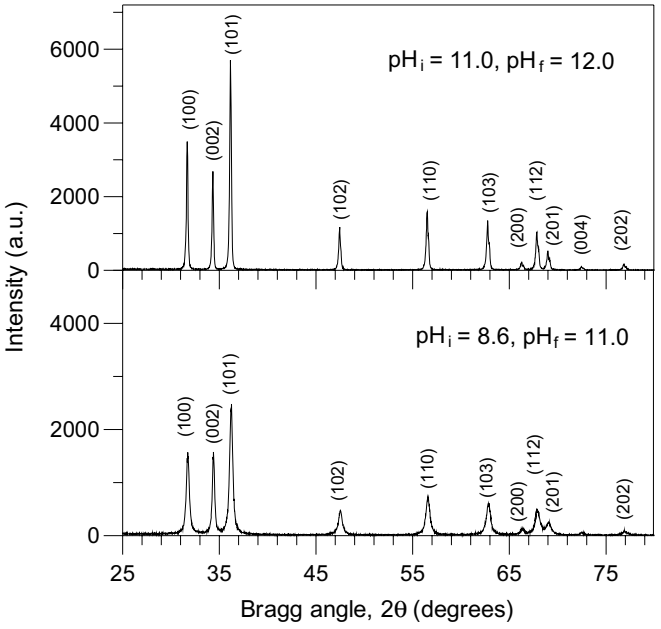

Fig. 2. XRD patterns of the ZnO nanostructures prepared with low (bottom) and high (top) differences of pH_i and pH_f values of the reaction mixture. The intensity of the diffraction peaks is greater when the difference between the initial and final pH values is smaller.

of all the samples were similar except the variation of the peak intensities due to the differences in growth conditions. From the figure, we can see that the crystallinity of the samples improved when the difference between the pH_i and pH_f is reduced, or in other words, when the morphology of the samples changed from particle-like to rod-like. Our EDS analysis revealed almost perfect stoichiometric

composition (Zn and O atomic ratio ≈1) for all the nanostructures with no presence of any other impurity.

The crystallinity and orientation of the nanostructures were further studied by HREM. The samples prepared with highest difference between the initial and final pH values ($pH_i = 8.6$ and $pH_f = 12.0$) revealed mostly rounded shaped nanoparticles of 30–70 nm diameter [12]. While the samples prepared with $pH_i = 8.6$ and $pH_f = 11.0$ revealed elongated particles, mostly along [0 0 2] growth direction, the sample prepared with $pH_i = 11.0$ and $pH_f = 12.0$ revealed well crystalline nanorods of about 170 nm average diameter and 2.5 μm average length. It is found that the nanorods grow along the [0 0 2] direction. In Fig. 3, the typical low and high resolution TEM images of the samples grown with different initial and final pH vales are presented. In fact, the samples grown with least difference between the initial and final pH values revealed single crystal structures with least structural defects and bulk-like lattice parameters.

In Fig. 4(a), typical Raman spectrum of an as-grown sample prepared with $pH_i = 11.0$ and $pH_f = 12.0$ (with uniform rod-like morphology) is presented. Raman spectrum of the nanostructure revealed 7 peaks at around 205, 332, 378, 409, 437, 556, 633 and 1110 cm^{-1}. While the 205

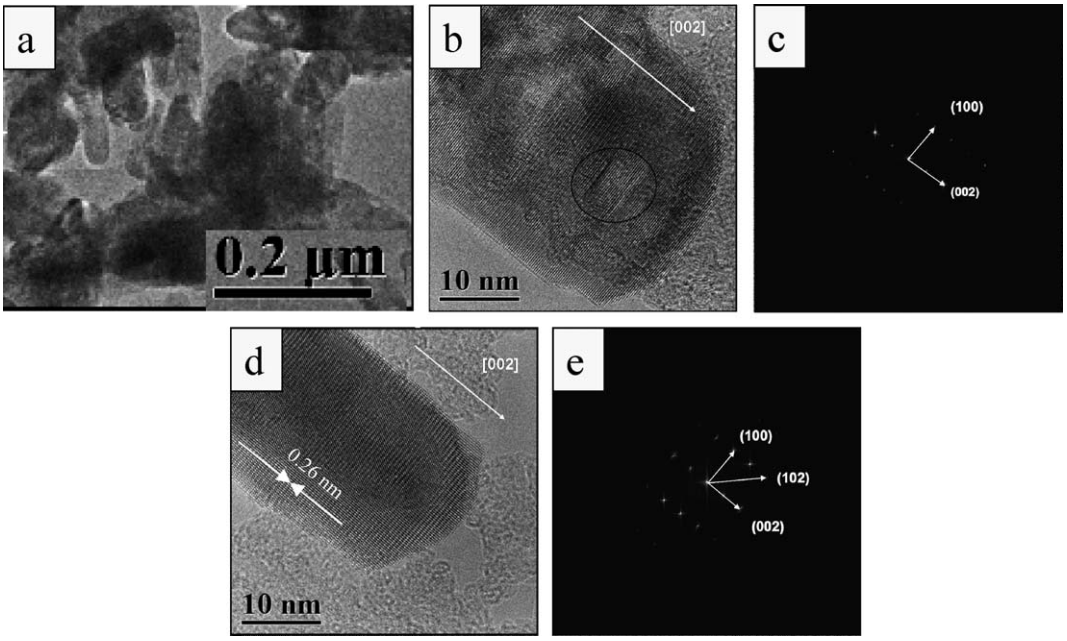

Fig. 3. Typical low and high resolution transmission electron micrographs of the ZnO nanostructures prepared with different initial and final pH values of the reaction mixture. While (a), (b) and (c) show the low magnification image, high resolution image and corresponding FFT for the sample prepared with $pH_i = 8.6$. and $pH_f = 11.0$ respectively, (d) and (e) show the typical HREM and corresponding FFT for the nanostructures prepared with $pH_i = 11.0$ and $pH_f = 12.0$ respectively. The presence of stacking fault in the earlier sample is shown by a circle.

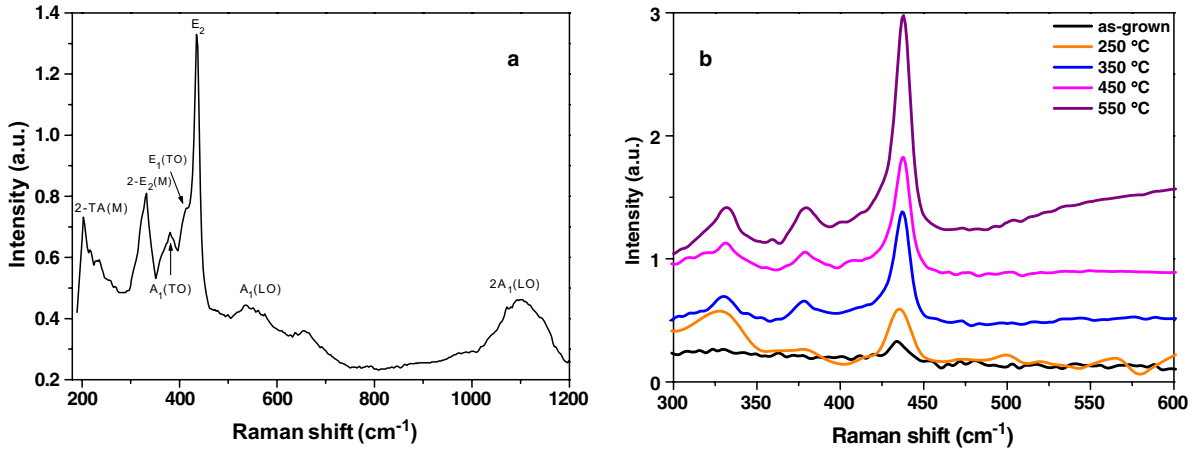

Fig. 4. (a) Typical Raman spectrum of the as-grown nanostructures prepared with optimum growth conditions; (b) Raman spectra of a nanostructured sample before and after air-annealing at different temperatures.

and 332 peaks are related to multiphonon process and have been assigned to the 2-TA(M) and 2-E_2(M) modes [13], the peaks around 378 and 409 cm^{-1} are the A_1(TO) and E_1(TO) modes respectively. The 437 cm^{-1} peak corresponds to the E_2 mode of wurtzite ZnO. While the origin of 635 cm^{-1} peak is not clear, the 556 and 1110 cm^{-1} peaks are assigned to the A_1(LO) mode and 2LO phonon respectively. Appearance of well-resolved Raman peaks related to multiphonon and resonance processes and the absence of E_1(LO) peak at 588 cm^{-1} related to oxygen deficiency indicate that the ZnO nanostructures are of very high quality. Air-annealing further improves the optical quality of the nanostructures, which can be observed in Fig. 4(b), where the Raman spectra of a typical sample before and after annealing at different temperatures are presented. From the figure, we can see a clear increase of the 437 cm^{-1} (E_2 mode) peaks intensity due to thermal annealing. Such an increase in Raman peak intensity indicates the reduction of growth-induced strain thus the improvement of crystalline quality.

The optoelectronic properties of the nanostructures and the effect of air annealing are further studied by measuring the PL spectra of the samples at room temperature. In Fig. 5, the PL spectra of the as-grown samples prepared at different initial and final pH values of the reaction mixture are shown. A broad and intense emission spreading from 450 to 650 nm along with a less intense band at around 385 nm can be seen from the spectra. While the 385 nm band is attributed to the band edge excitonic luminescence of ZnO [14–16], the broad band in the visible region is generally believed to be associated with intrinsic defects in nominally undoped ZnO [17–22].

The broad emission near 520 nm in ZnO is often referred as the green emission, while other broad emission at around 580 nm is referred as yellow emission [17–20]. The origins of the visible emissions in ZnO are controversial. Nevertheless it is probably most popular to assign them to singly ionised oxygen vacancy [21,22] and interstitial O_i [23,24] respectively. To be more specific, the green emission is attributed to the radiative recombination of a delocalised electron close to the conduction band with deeply trapped hole in V_0^+ center, the yellow emission is attributed to the radiative recombination of a similar electron with deeply trapped hole in O_i^- center [24]. We believe, the presence of both type of defects in our samples is responsible for the observed broad visible PL band. This can be further verified from the PL spectra of samples annealed in air at different temperatures.

In Fig. 6, the PL spectra for a typical sample (prepared with $pH_i = 9.0$ and $pH_f = 11.0$ of the reaction mixture), as-prepared and annealed at different temperatures in air are presented. Among these samples, the strongest excitonic emission is achieved for the sample annealed at 250 °C. This suggests that 250 °C is the optimum annealing temperature to minimize the defects acting as non-radiative cen-

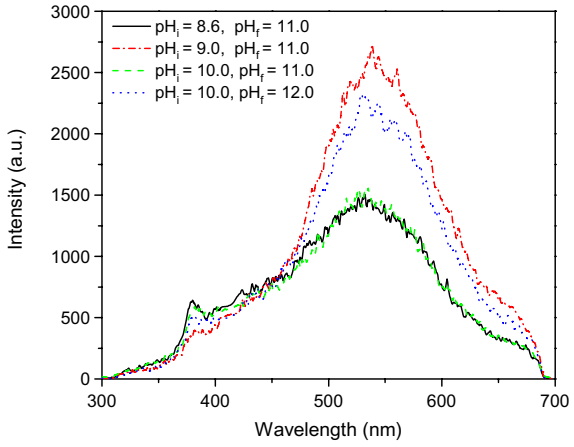

Fig. 5. PL spectra of as-grown ZnO nanostructures prepared with different initial and final pH values of the reaction mixture.

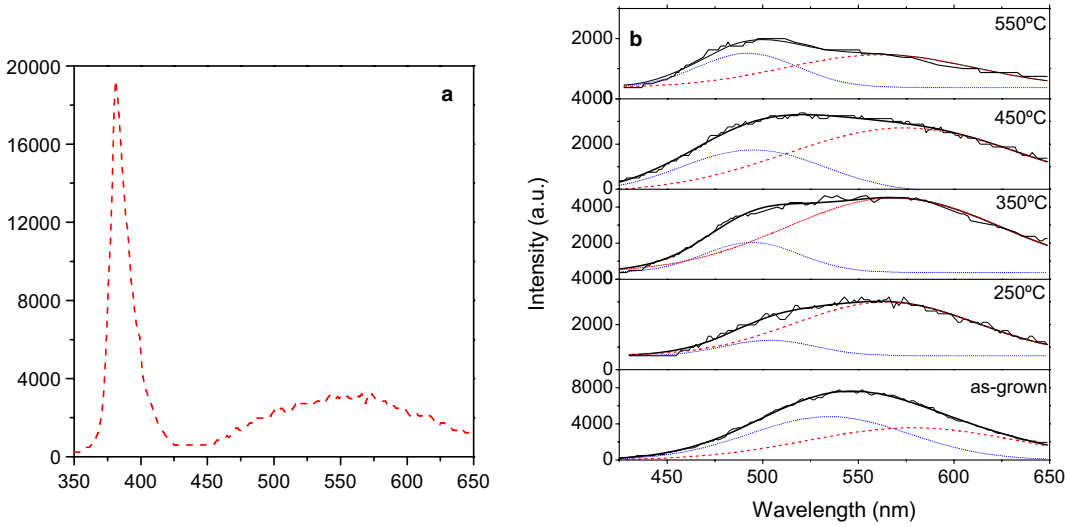

Fig. 6. PL spectra of the sample prepared with $pH_i = 10.0$ and $pH_f = 12.0$, (a) annealed at different temperatures; (b) de-convoluted defect bands of corresponding samples.

ters of excitons in our ZnO samples. Annealing in air also reduces the visible defect luminescence, which might be due to the improvement of sample stoichiometry. The presence of both green and yellow emissions can be seen through the de-convolution of the defect-band in Fig. 6(b). On increasing the annealing temperature, the position of the green emission shifted from 535 to 500 nm and its intensity decreased. The air-annealing treatment also causes a shift of the yellow band position from 588 nm to 565 nm and reduction of its intensity. The shifts of these two visible PL bands might be due to changes in the local environments of the defect centers in the samples due to annealing [17,21].

As the origin of these tow bands are opposite in nature, a competitive evolution of the two emissions is likely to occur. Annealing in air usually reduces oxygen vacancies while increases the amount of oxygen interstitials in the sample. Form room temperature to 350 °C, the intensity evolution of these two bands is of reciprocal nature; i.e., the relative intensity of one increases in expense of other. This indicates a reduction of oxygen vacancies and increase of oxygen interstitials in the sample. It also suggests that annealing at low temperature enhances this process. Above 350 °C, the relative intensity variation of these two bands becomes arbitrary. One possible reason accounts for this behavior may be that oxygen starts to escape from the sample at high temperature, thus causing a drastic change in the local environments of the defect centers in the sample.

4. Conclusions

ZnO nanostructures with different morphologies could be prepared thorough a low-temperature hydrothermal process by simply adjusting the initial and final pH values of the reaction mixture. By varying the pH values of the reaction mixture, the rate of nucleation and growth of the nanostructures could be controlled. The synthesized nanostructures were of good structural and optical qualities. The samples prepared with lowest difference between the initial and final pH values were of best structural and optical qualities. Annealing the samples in air, apart from reducing the growth induced strain, reduces the electronic defects responsible for the visible defect luminescence in ZnO. It is found that 250 °C is the optimum annealing temperature to achieve strongest excitonic emission in ZnO nanostructures while to suppress the visible defect PL.

Acknowledgements

We thank E. Aparicio Ceja, CCMC-UNAM for her help in taking the XRD spectra of the samples. The work is partially supported by CONACyT, Mexico (Grant No. 4626) and UC-MEXUS–CONACyT (Grant No. CN-05-215).

References

[1] M.H. Huang, S. Mao, H. Feick, H.Q. Yan, Y. Wu, H. Kind, E. Weber, R. Eusso, P. Yang, Science 292 (2001) 1897.
[2] E. Comini, G. Fagila, G. Sberveglieri, Z. Pan, Z.L. Wang, Appl. Phys. Lett. 81 (2001) 1869.
[3] X.D. Bai, P.X. Gao, Z.L. Wang, E.G. Wang, Appl. Phys. Lett. 82 (2003) 4806.
[4] U. Rau, N. Schmidt, Thin Solid Films 387 (2001) 141.
[5] V.A.L. Roy, A.B. Djurisic, W.K. Chan, J. Gao, H.F. Lui, C. Surya, Appl. Phys. Lett. 83 (2003) 141.
[6] Y. Zhang, H. Jia, L. Xuhubi, X. Chen, D. Yu, W. Rongming, J. Phys. Chem. B 107 (2003) 8289.
[7] P.X. Gao, Z.L. Wang, J. Phys. Chem. B 108 (2004) 7534.
[8] H.T. Ng, B. Chen, J. Li, J. Han, M. Meyyaooan, J. Wu, S.X. Li, E.E. Haller, Appl. Phys. Lett. 82 (2003) 2023.
[9] J. Jiansheng, G. Wang, Q. Wang, Y. Chen, X. Han, X. Wang, J.G. Hou, J. Phys. Chem. B 108 (2004) 11976.
[10] J. Wang, L. Gao, J. Mater. Chem. 13 (2003) 2551.
[11] B. Liu, H.C. Zeng, J. Am. Chem. Soc. 125 (2003) 4430.
[12] U. Pal, P. Santiago, J. Phys. Chem. B 109 (2005) 15317.
[13] J.M. Calleja, M. Cardona, Phys. Rev. B 16 (1997) 3753.
[14] J.B. Baxter, F. Wu, E.S. Aydil, Appl. Phys. Lett. 83 (2003) 3797.
[15] C. Jiang, W. Zhang, G. Zou, W. Yu, Y. Qian, J. Phys. Chem. B 109 (2005) 1361.
[16] D. Banerjee, J.L. Lao, D.Z. Wang, J.Y. Huang, D. Steeves, B. Kimball, Z.F. Ren, Nanotechnology 15 (2004) 404.
[17] K. Vanhusden, C.H. Seager, W.L. Warren, D.R. Tallant, J.A. Voigt, Appl. Phys. Lett. 68 (1995) 403.
[18] H.C. Ong, G.T. Du, J. Cryst. Growth 265 (2004) 471.
[19] S.A. Studenikin, N. Golego, M. Cocivera, J. Appl. Phys. 84 (1998) 2287.
[20] B. Lin, Z. Fu, Y. Jia, Appl. Phys. Lett. 79 (2001) 943.
[21] K. Vanheusden, W.L. Warren, C.H. Seager, D.R. Tallant, J.A. Voigt, B.E. Gnade, J. Appl. Phys. 79 (1996) 7983.
[22] K. Osaga, K. Sakurai, S. Fujita, S. Fujita, K. Matsushige, J. Cryst. Growth 214&215 (2000) 312.
[23] M. Liu, A.H. Kitai, P. Mascher, J. Lumin. 54 (1992) 35.
[24] X.L. Wu, G.G. Siu, C.L. Fu, H.C. Ong, Appl. Phys. Lett. 78 (2001) 2285.